

Novel magnetic field tuning of quantum spin excitations in a weakly coupled $S = 1/2$ Heisenberg spin chain as seen from NMR

Long Ma¹, Z. Wang¹, L. Hu^{1,*}, Z. Qu^{1,†}, N. Hao¹, and Li Pi^{1,2‡}

¹Anhui Province Key Laboratory of Condensed Matter Physics at Extreme Conditions, High Magnetic Field Laboratory, Chinese Academy of Sciences, Hefei 230031, China

²Hefei National Laboratory for Physical Sciences at the Microscale, University of Science and Technology of China, Hefei 230026, China

(Dated: September 19, 2019)

We report our NMR study of the spin excitations in the quasi-one dimensional (1D) $S = 1/2$ quantum magnet $\text{CH}_3\text{NH}_3\text{Cu}(\text{HCOO})_3$ lying in the 1D-3D dimensional crossover regime with Dzyaloshinskii-Moriya (DM) interactions. Above T_N , the spinon excitation is observed from the constant $1/T_1$ at low temperatures contributed from the staggered spin susceptibility. At low temperatures well below T_N , the $1/T_1$ begins to flatten out under weak magnetic fields. With the increasing field intensity, $1/T_1$ tends to show a power-law temperature dependence gradually, with the index increasing from zero to ~ 3 , and finally ~ 5 , which are the respective typical characteristic for the dominating two-magnon Raman process and three-magnon scattering contributions to the nuclear relaxation in a conventional 3D magnet. A possible physical mechanism for this novel magnetic field tuning of quantum spin excitations related with the enhanced effective staggered field created by the DM interactions under magnetic field is discussed.

PACS numbers: 75.10.Pq, 75.40.Gb, 76.60.-k

In low-dimensional (low-D) magnets, the enhanced quantum fluctuations lead to novel states of matter, exotic elementary excitations with integer or fractional quantum numbers, as well as fascinating critical phenomena¹⁻⁴. Studies on the quantum-mechanical effects in low-D magnets have triggered enormous and un-failing research interest in the condensed matter society, and have profound influences on the understanding of high- T_C superconductivity, fractional quantum Hall effect, and other strongly-correlated electron systems⁵⁻⁸. Among others, a prototypical example is the one-dimensional $S = 1/2$ Heisenberg antiferromagnetic spin chain (HAFC), where the strong quantum fluctuations prohibit any possible Néel order even at zero temperature limit⁹. This spin system has received long-lived research interest since it's analytically solvable¹⁰, provides a rare opportunity for rigorous comparison between the experimental results and theoretical approaches^{11,12}, and gives a valuable test of the reliability of the theoretical approximation.

The $S = 1/2$ HAFC shows a gapless spin excitation spectrum with a large area of continuum, and the excitation quasiparticle is fractionalized with $S = 1/2$ (spinon)¹³⁻¹⁵. When the inter-chain coupling is included, 3D long range Néel order will be restored at sufficiently low temperatures. The effective staggered field resulting from the inter-chain coupling confines pairs of the quantum spinons into classical magnons, the Goldstone mode of the translational symmetry breaking. From the spin dynamics, the spin excitation spectrum of the quasi-1D spin chain system is dominated by the sharp dispersive spin waves at the low energy region and the continuum spectrum formed by multi-spinon excitations at higher energies¹⁶. The longitudinal mode of the spin wave excitation is proposed theoretically based on mean-

field or Random phase approximations (RPA)^{17,18}. This is substantially different with the spin excitations in the conventional 3D antiferromagnets, which is mainly contributed by the well-defined transverse spin waves. By tuning the inter-chain coupling, the dimensional crossover from the critical quantum disordered 1D spin system to the classical 3D magnets occurs, which is important for understanding the semiclassical behavior induced by underlying quantum fluctuations in the materials in the real 3D world.

The quasi-1D HAFC is realized in several compounds with very different magnetic coupling strength, KCuF_3 ^{16,19,20}, Sr_2CuO_3 and SrCuO_2 ²¹⁻²³, $\text{BaCu}_2\text{Si}_2\text{O}_7$ ²⁴⁻²⁶ et al. The dimensionality can be measured by the ratio between the intra-chain coupling J and the Néel ordered temperature T_N , also the ordered moment m_0 , as the T_N is roughly proportional to the inter-chain coupling strength and the quantum fluctuations can strongly suppress the static moment in the ordered state. For KCuF_3 , $J = 17$ meV, $T_N = 39$ K ($J_\perp/J \sim 0.084$), and $m_0 = 0.5\mu_B$ ^{19,20}, which is close to the 3D spin system. The nearly ideal 1D-character is realized in Sr_2CuO_3 and SrCuO_2 , with a strong intra-chain exchange interaction energy J of ~ 190 meV and ~ 181 meV, a low T_N of 5.4 K and 2 K ($J_\perp/J \sim 7 \times 10^{-4}$ and 2.5×10^{-4}), and a very small ordered moment both with the order of $< 0.1\mu_B$ (close to or below the detecting limit), respectively²¹⁻²³. The $\text{BaCu}_2\text{Si}_2\text{O}_7$ lies on the dimensional crossover regime, where the J equals to 24.1 meV and the antiferromagnetic transition occurs at $T_N = 9.2$ K ($J_\perp/J \sim 0.011$) with a static ordered moment of $0.15\mu_B$ (Refs. [24-26] and therein). The novel longitudinal mode is evident by inelastic neutron scattering with a reduced life time due to the decay into two transverse spin waves in KCuF_3 ^{27,28}, consistent

with the theoretical predictions. The $\text{BaCu}_2\text{Si}_2\text{O}_7$ spin system locates on the 1D to 3D crossover regime with an enhanced quantum fluctuations, thus the longitudinal mode should be stronger. Surprisingly, a single broad continuum is observed in the longitudinal spin excitation spectrum, indicating the absence of the longitudinal mode^{26,29}. This contradiction should be attributed to the ignorance of the correlation effects in the mean-field and RPA approach. Unusual excitations is observed in Sr_2CuO_3 recently by electron spin resonance³⁰, which may be related to interactions between the Goldstone magnons and the amplitude fluctuations of the order parameter. As a result, the quantum correlation effects should play an important role in the dominance of the spin excitations when the spin system moves closer to the quantum critical point. According to our knowledge, satisfactory theory describing the spin systems near the 1D-3D dimensional crossover region is still highly lacked.

Nuclear magnetic resonance (NMR), mainly detecting the on-site hyperfine field and its fluctuations resulting from the electron spins via the hyperfine coupling, is a powerful local probe accessing the magnetic susceptibility, magnetic order as well as spin dynamics near the quantum critical point in weakly coupled quasi-1D antiferromagnets. Several NMR results concerning the Luttinger physics in quasi-1D quantum antiferromagnets tuning by the applied magnetic field are reported³¹⁻³⁴, important for the relative research on quantum criticality behaviors. In this paper, we report our NMR study on the $\text{CH}_3\text{NH}_3\text{Cu}(\text{HCOO})_3$ (Cu-MOF) quantum magnet lying on the 1D-3D crossover regime. The G -type antiferromagnetic order with spin canting is proposed from the spectral analysis. Above T_N , free spinons are observed from the constant $1/T_1$ contributed from the staggered spin susceptibility. Below T_N , the $1/T_1$ begins to flatten out at low temperatures at the weak magnetic field side. By increasing the field intensity, the $1/T_1$ gradually shows a power-law temperature dependence at low temperatures with the index of ~ 3 to ~ 5 , corresponding to the two-magnon dominant and three-magnon dominant contributions to the nuclear relaxation in a classical 3D magnet. This novel magnetic field tuning of the quantum magnetic fluctuations in the ordered state is possibly related with the enhanced effective staggered field generated by the Dzyaloshinskii-Moriya (DM) interactions under magnetic field. This newly discovered phenomena should be fresh physical inputs for constructing proper theoretical models.

High quality Cu-MOF single crystals are synthesized under the solvothermal conditions³⁵. Single crystals with typical dimensions of $2 \times 2 \times 1.5 \text{ mm}^3$ are chosen for our NMR study. Our NMR measurements are conducted on the ^1H nuclei ($\gamma_n = 42.5759 \text{ MHz/T}$, $I = 1/2$) with a phase-coherent NMR spectrometer. The spectra are obtained by summing up the spin-echo intensities as a function of frequency. The spin-lattice relaxation rates are measured by a conventional inversion-recovery method, and fitting the nuclear magnetization to the standard re-

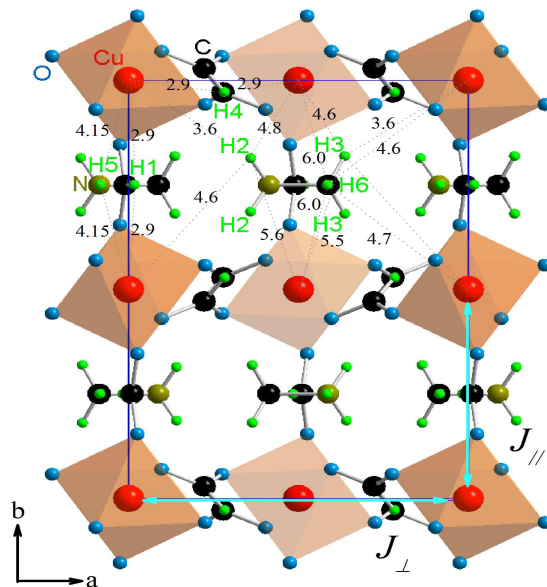


FIG. 1: (color online) The crystal structure of $\text{CH}_3\text{NH}_3\text{Cu}(\text{HCOO})_3$ viewed from c -axis. The CuO_6 octahedron with obvious Jahn-Teller distortion is shown by the orange polyhedra. The crystallographically inequivalent positions of hydrogen is marked with H_1 , H_2 to H_6 , whose distance with the nearest Cu^{2+} neighbours is also shown by the dotted line and numbers in angstrom.

laxation curve for $I = 1/2$. All the data are collected during the warming-up process for self-consistence.

The Cu-MOF crystallizes in a orthorhombic structure with space group $Pnma$ ($Z = 4$). Fig.1 shows the detailed structure of Cu-MOF, with the CuO_6 octahedron shown by the orange polyhedra. The structure shows a distorted perovskite-like (with a general chemical formula ABX_3) characteristic, with the A sites occupied with the $(\text{CH}_3\text{NH}_3)^+$ cations and $(\text{HCOO})^-$ anions occupying the X sites bridging the magnetic interactions between the Cu^{2+} sitting on the B sites. The $3d^9$ configuration of Cu^{2+} in the cubic crystal field makes the Cu-MOF be a Jahn-Teller active system, leading to local distortions in the crystal structure and the orbital ordering, which is supported by very different Cu-O bonds' length. Based on the Goodenough-Kanamori-Anderson (GKA) rules³⁶, shorter Cu-Cu distance along b -axis and more significant antiferromagnetic interactions between the half-filled $d_{x^2-y^2}$ through the $[\text{HCOO}]^-$ anions may give much stronger antiferromagnetic coupling along b -axis³⁵, and a weaker ferromagnetic coupling in the ac -plane. Experimentally, both the broad Bonner-Fisher peak at $T \sim 45 \text{ K}$ shown in the temperature dependence of the susceptibility and the obviously anisotropic responds of the magnetization to the applied field confirm the quasi-1D magnetism in Cu-MOF³⁵. This mechanism is very similar to what occurs in the model spin system KCuF_3 with a similar 3D structure²⁰. The intra-chain (along b -axis) coupling J is estimated to be $\sim 6 \text{ meV}$ from

Bonner-Fisher fitting to the susceptibility, and the T_N is ~ 4 K at low magnetic field³⁵. Based on the mean-field theory, the ratio between the inter- and intra-chain coupling is estimated to be $J_{\perp}/J \sim 0.02$. Therefore, the spin system in Cu-MOF locates on the 1D-3D crossover regime, between $\text{BaCu}_2\text{Si}_2\text{O}_7$ and KCuF_3 .

We conduct our NMR study on Cu-MOF via the ^1H site, as strong wipe-out effect of $^{63,65}\text{Cu}$ nuclei make the signals undetectable due to too fast spin-spin relaxations on the magnetic sites. Six crystallographically inequivalent positions of hydrogen exist in Cu-MOF, which is marked with H_1, H_2 to H_6 in Fig.1 and the distance between them and their nearest Cu^{2+} neighbours is also shown. In this magnetic insulator, the hyperfine coupling is mainly contributed from the dipolar interactions between the nuclear spins and electron orbitals and spins, which is very sensitive to the distance between the nuclei and magnetic ions. Obviously, the H_1 and H_4 sites from $[\text{HCOO}]^-$ anions locate much nearer to Cu^{2+} sites. Additionally, the $[\text{HCOO}]^-$ anion bridging the magnetic interactions, has chemical bonds with Cu^{2+} sites, while the $(\text{CH}_3\text{NH}_3)^+$ cations link with the framework via much weaker H-bonds. Thus, the hyperfine coupling of H_1 and H_4 sites from $[\text{HCOO}]^-$ anions should be much stronger than the other four hydrogen sites.

Typical frequency-swept NMR spectra at various temperatures are shown in Fig.2 (a) and (c) for both field directions. The spectrum is composed by a single peak at higher frequency and a group of peaks near the Larmor frequency which overlap with each other at high temperatures and separate from others with the sample cooling down as a result of the increased spin susceptibility. At $T = 6$ K above T_N , six well defined Lorentz peaks are identified (See Fig.2 (b)), corresponding respectively to the six crystallographically inequivalent hydrogen sites. Based on the above discussions of the hyperfine coupling shown above, we assign the *A* and *F* peaks to the hydrogen in $[\text{HCOO}]^-$ anions, and the other four peaks to the hydrogen in $(\text{CH}_3\text{NH}_3)^+$ cations. The Knight shifts (defined as $K = (f - \gamma_n B_0)/(\gamma_n B_0)$, where the f denotes the actual resonance frequency, and B_0 the applied magnetic field) of different peaks show similar temperature dependence, all reflecting the bulk spin susceptibility. We select the peak with the strongest hyperfine coupling (marked with the thick gray line in Fig.2 (a) and (c)) to study the magnetic properties in order to gain a better sensitivity. The temperature dependence of the Knight shift of the *F* peak and dc susceptibility in the paramagnetic state is shown in Fig.2 (d). With the sample cooling down, the Knight shifts show a Curie-Weiss upturn at high temperatures, and show a broad peak at $T_{max} \sim 45$ K, consistent with the dc susceptibility. Based on the equation $T_{max} = 0.641J_{//}$ expected for $S = 1/2$ Heisenberg chains³⁷, the intra-chain coupling $J_{//}$ is estimated to be ~ 6 meV, consistent with previous results. For temperatures below $T \sim 18$ K, the Knight shifts also show the upturn behavior as seen from the dc susceptibility, indicating an intrinsic enhanced spin sus-

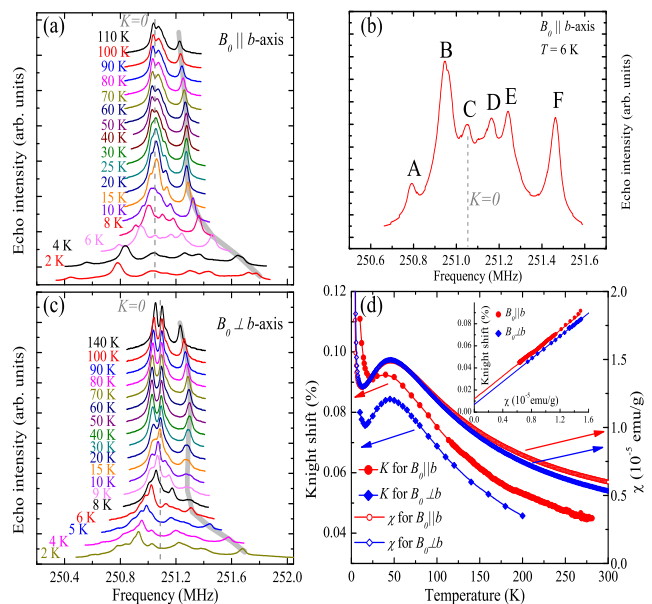


FIG. 2: (color online) (a): The ^1H NMR spectra under different temperatures with a 5.9 T magnetic field applied along the crystalline b -axis. The vertical dashed line show the Larmor frequency $\gamma_n B_0$. (b): An enlarged version of the spectrum at $T = 6$ K in (a). (c): Temperature dependence of ^1H NMR spectra with $B_0 \perp b$ -axis. (d): The Knight shift and dc susceptibility versus temperature for both field directions. For the susceptibility measurement, a field of 200 Oe is applied, and the data are collected with the sample warming up after a zero field cooling (ZFC) process. Inset: the Knight shift as a function of dc susceptibility with the temperature as an explicit parameter (See the text).

ceptibility in Cu-MOF. This behavior is related to the DM interactions in this sample due to the lack of inversion symmetry center, which will be discussed later. As $K = K_{spin} + K_{orbit} = A_{hf} \chi_{spin} + K_{orbit}$, we can extract the diagonal element of the hyperfine coupling constant tensor A_{hf} from the slope of the line by plotting the Knight shift versus dc susceptibility with temperature as an explicit parameter (See Fig.2(d) inset, also called Clogston-Jaccarino plot³⁸). The linear fittings give the hyperfine coupling $A_{hf}^{bb} = 1.254$ kOe/ μ_B and $A_{hf}^{aa/cc} = 1.252$ kOe/ μ_B , which is nearly isotropic.

The spectral broadening below $T = 6$ K results from the emergence of magnetic order. In Fig.3 (a) and (b), we show the spectra at $T = 2$ K under different field intensities with $B_0 \parallel b$ and $B_0 \perp b$ -axis. By increasing the field intensity, the spectra are broadened and a slight line splitting for the peak from the $[\text{HCOO}]^-$ anions noted by the gray line is observed for $B_0 > 3.7$ T, which is more clear for $B_0 \parallel b$ (See Fig.3 (a) and (b)). We plot the internal field calculated from the frequency shift $f - \gamma_n B_0$ versus field in Fig.3 (c) and (d). For the line shift and broadening with a paramagnetic origination, the internal field is proportional to the magnetic field, which is shown by the dashed line. However, this is obviously not

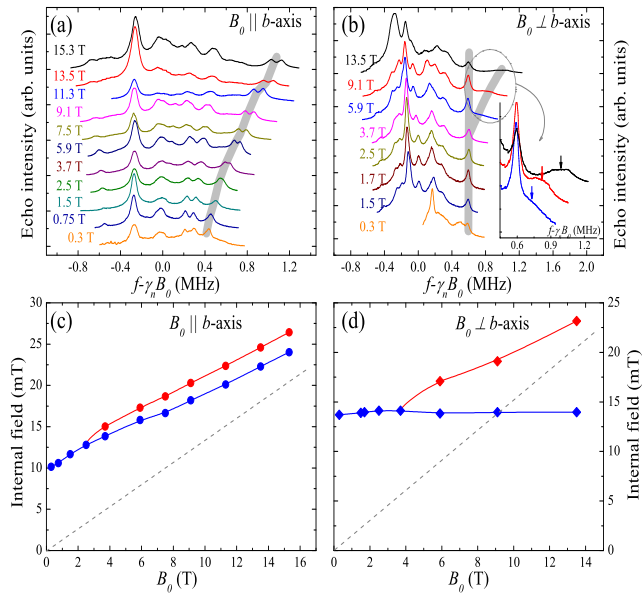


FIG. 3: (color online) The spectra at $T = 2$ K for different field intensities with the $B_0 \parallel b$ (a) and $B_0 \perp b$ -axis (b), respectively. The gray lines show the change of the relative frequency shift of the studied signal peak. The enlarged version of the field induced spectral splitting is shown in (b) inset. (c) and (d): The field dependence of the internal field calculated from $H_{in} = \Delta f / \gamma_n$ of the peaks denoted in (a) and (b) for both directions. The field dependence of the internal field for the paramagnetic state is shown by the dashed line.

the actual situation observed in this sample. The field dependence gives an intercept to a nonzero internal field at $B_0 = 0$, which is strong evidence for the magnetically ordered ground state.

The magnetic structure with a G -type antiferromagnetism with spin-canting is suggested from the spectra. At $T = 2$ K well below T_N with the applied field less than 3.7 Tesla, the main characteristic of the spectrum is maintained as compared with that in the paramagnetic phase (data not shown), and no additional line splitting due to the setup of the antiferromagnetic order is observed. This is very different from the ordinary antiferromagnetic order³⁹. Two scenarios can be proposed: One is the very small magnetic moment; the other one is the cancelation of the hyperfine field on the ^1H sites from the magnetic moments located at the two nearest Cu^{2+} neighbours. At $B_0 = 1.5$ T, the studied peak at $T = 2$ K is broadened by ~ 50 kHz as compared with that at $T = 5$ K well above T_N . By the moderate hyperfine coupling constant discussed above, the upper limit of the ordered moment is estimated to be $0.0094\mu_B$. In the nearly ideal quasi-1D spin chain Sr_2CuO_3 , the ordered moment is $\sim 0.06\mu_B$, which is reduced by strong quantum fluctuations. According to the mean-field theory¹⁷, the ordered moment is proportional to $\sqrt{J_\perp/J_\parallel}$. Thus, for the present Cu-MOF located at the 1D-3D crossover regime, the $0.0094\mu_B$ ordered moment size is obviously

too small to be reasonable. Thus, our results point to the second one.

Every proton in the $[\text{HCOO}]^-$ anions has two nearest Cu^{2+} neighbours along all the three crystalline directions. The angle of $\text{Cu-H}_1\text{-Cu}$ and $\text{Cu-H}_4\text{-Cu}$ is $\sim 161^\circ$ and $\sim 155^\circ$, far from the exact geometric center between the two adjacent magnetic sites. The Jahn-Teller distortion again lowers the crystalline symmetry³⁵. Thus, the cancelation of the internal field occurs only in ordered states with a G -type configuration, where the magnetic moments order antiferromagnetically for all the three directions. However, this type of antiferromagnetic order contradicts with the ferromagnetic interactions in the ac -plane as discussed above according to the GKA rules³⁶. The discrepancy may be related with the emergence of complex DM interactions, and further identification of the antiferromagnetic order and determination of the magnetic interaction strength is needed.

The increasing Knight shifts at low temperatures indicate that the upturn behavior of the dc susceptibility results from intrinsic enhanced spin susceptibility instead of the trivial impurity effect. The ^1H peaks shift further with respect to the Larmor frequency even in the antiferromagnetic ordered state, which is distinct with the ordinary antiferromagnets. In Cu-MOF, the $(\text{CH}_3\text{NH}_3)^+$ cations sitting on the A sites lack the spatial-inversion symmetry, resulting in the DM interaction between magnetic sites, which is important for the appearance of multiferroic behavior in its counterpart $\text{CH}_3\text{NH}_3\text{Co}(\text{HCOO})_3$ ⁴⁰. Thus, the ^1H sites only pick the component of hyperfine field resulting from canted static moment, while that from the antiferromagnetic arrangement of moments is canceled out.

The enhancement of the internal field and line splitting due to applied magnetic field reflect the tilting magnetic moment and spin reorientations. With $B_0 \parallel b$, the internal field shown by the original peak at low frequency increases with field strength as shown in Fig.3(c), while that for $B_0 \perp b$ remains nearly constant. The anisotropy again demonstrates the quasi-1D magnetic behavior induced by strong axial anisotropic magnetic interactions. This is consistent with the field dependence of the magnetization at $T = 2$ K.

Next, we concentrate on the spin excitation and its evolution under magnetic field. The spin-lattice relaxation rate $1/T_1$ is a measure of the dynamic spin susceptibility, whose temperature and field dependence reveal the nature of spin fluctuations in the strongly-correlated systems. In Fig.4, we show the temperature dependence of $1/T_1$ above T_N at various magnetic field intensities for both $B_0 \parallel b$ (a) and $B_0 \perp b$ -axis (b). For $B_0 = 0.75$ T $\parallel b$ -axis, the $1/T_1$ shows a nearly temperature-independent behavior from T_N to $T \sim 20$ K, which is followed by the linear temperature dependence denoted by the gray line at higher temperatures. With the field intensity increased, besides the temperature dependence of $1/T_1$ described above, a "hump" structure is observed at temperatures ranged from $T = 40$ K to 60 K. The intensity

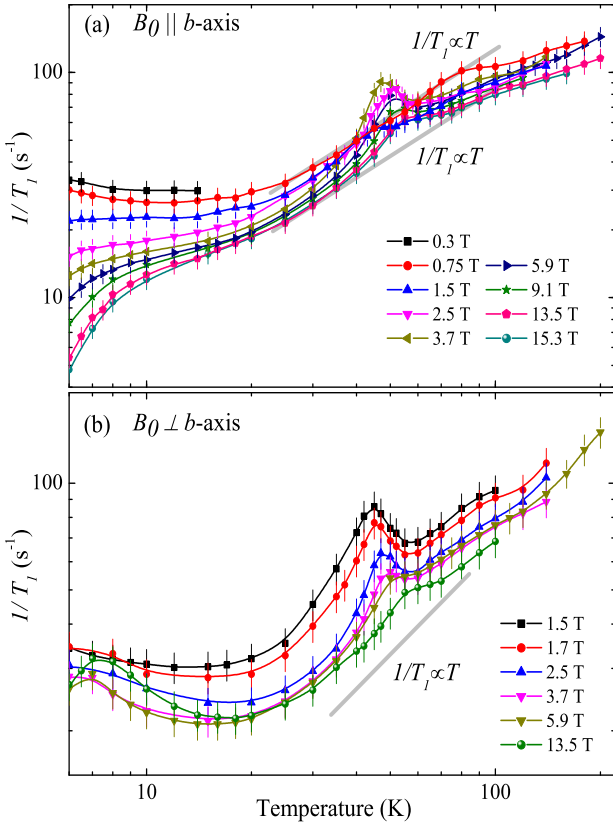


FIG. 4: (color online) The spin-lattice relaxation rate $1/T_1$ in the paramagnetic state ($T \geq 7$ K) as a function of temperature under different field intensities for $B_0 \parallel b$ (a) and $B_0 \perp b$ -axis (b). Solid lines show the linear temperature dependence of $1/T_1$.

of the "hump" is enhanced firstly, reaches its maximum at $B_0 = 3.7$ T, and is suppressed with further increased field intensity. For $B_0 \perp b$ -axis, similar $1/T_1$ behavior is observed (Fig.4(b)).

The $1/T_1$ behavior shown in Fig.4(a) can be completely understood for this quasi-1D HAFC system. For the applied magnetic field along z direction, the $1/T_1$ can be expressed as

$$1/T_1 = \gamma_n^2 [\langle (\mu_0 h_x)^2 \rangle + \langle (\mu_0 h_y)^2 \rangle] \times \frac{\tau_c}{1 + \omega_L^2 \tau_c^2}$$

, where the the first part before " \times " describes the spin fluctuations at both the directions perpendicular to the applied field⁴¹. The second part, where τ_c and ω_L denote the typical time scale of the electron system and the nuclear Larmor frequency respectively, undergoes a maximum for $\tau_c = 1/\omega_L$. Thus, we attribute the "hump" structure to the slow dynamics of the spin system.

The scaling theory for the $S = 1/2$ HAFC⁴² predicts that the staggered spin susceptibility contributed by spinon excitations dominates the $1/T_1$ at low temperatures ($T \ll J/k_B$), leading to a constant $1/T_1$. While, the uniform spin susceptibility dominating the $1/T_1$ at

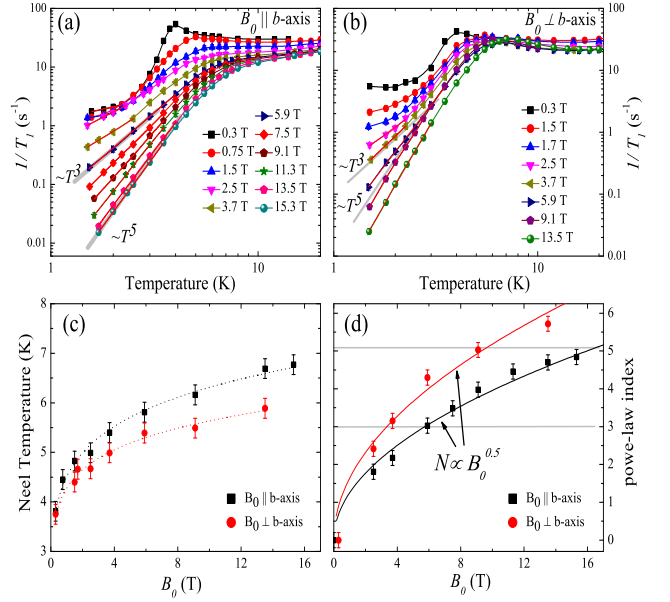


FIG. 5: (color online) The spin-lattice relaxation rate $1/T_1$ below $T = 20$ K, as a function of temperature under different field intensities for $B_0 \parallel b$ (a) and $B_0 \perp b$ -axis (b). Solid lines show the T^3 and T^5 temperature dependence of $1/T_1$. Red straight lines are power-law fits to the $1/T_1$. (c): The field dependence of the Néel temperature. The dotted lines are guides to the eye. (d): The power-law index N as a function of magnetic field. Solid lines are fits to the function $N = A \times \sqrt{B_0}$, where A is the fitting parameter.

higher temperatures ($T < J/k_B$), results in a linear temperature dependence of $1/T_1$. Thus, our data fit quite precisely with this theory, and provide strong evidence for the spinon excitations at low temperatures, and again demonstrate the 1D character of this molecule magnet⁴³. This result is obviously very different with the classical spin chains, where the $T^{-3/2}$ temperature dependence of $1/T_1$ is theoretically predicated⁴⁴.

The inter-chain coupling results in the 3D Néel order below T_N . In Fig.5 (a) and (b), we show the temperature dependence of $1/T_1$ below T_N for both field directions to study the field dependence of the spin excitations in the ordered state. For $B_0 = 0.3$ T, the nearly-constant $1/T_1$ decreases sharply below T_N , and begins to flatten out below $T \sim 3$ K for both field directions. With increasing the field intensity, we observe a power-law temperature dependence of the $1/T_1$ for temperatures well below T_N , and further plot the power-law index versus field intensity in Fig.5 (d). For a conventional 3D antiferromagnet, the $1/T_1$ is mainly contributed by the scattering of nuclear spins by magnons. Theoretical calculations⁴⁵ predict a T^3 -dependence of $1/T_1$ for the two-magnon Raman process, and a T^5 -dependence of $1/T_1$ for the three-magnon process for $T \gg \Delta$ (Δ is the excitation gap of magnons).

The evolution of the low-energy spin excitations observed in $1/T_1$ under magnetic field should be related with the enhanced effective local transverse staggered

field raised by the DM interaction with the increasing field. In the well-known HAFC systems without DM-interactions such as KCuF_3 , $\text{BaCu}_2\text{Si}_2\text{O}_7$, Sr_2CuO_3 and SrCuO_2 , the low-lying spin excitations for the magnetically ordered state are dominated by the spin waves, and free spinons are observed at a higher energy region with a finite gap as seen from Raman scattering and neutron scattering studies^{46–48}. According to the mean-field theory, the spinon excitation gap size Δ is proportional to $h^{2/3}$, where h denotes the effective staggered field¹⁷, with the intensity determined by the inter-chain coupling and the orientation along the antiferromagnetic arrangement of the moment.

For the HAFC systems with strong DM interactions and very weak inter-chain coupling, the effective staggered field can be generated by the DM interaction. In copper benzoate $\text{Cu}(\text{C}_6\text{H}_5\text{COO})_2 \cdot 3\text{H}_2\text{O}$, quasi-1D magnetic behavior is observed from susceptibility, ESR and NMR measurements⁴⁹, where the inter-chain coupling is very weak. The effective transverse staggered field is generated by the combined effect of anisotropic g -tensor and DM interactions. From theoretical results^{50–52}, the HAFC with DM interactions under magnetic field can be mapped to simple Heisenberg spin chains with an effective staggered field. The intensity of staggered field is proportional to the applied external field and the direction is determined by $\vec{B}_0 \times \vec{D}$ (\vec{D} is the DM \vec{D} vector). This theory is evident to be successful in describing the field induced spin wave excitation gap in copper benzoate and copper pyrimidine dinitrate^{53,54}.

In the present Cu-MOF sample, the DM interactions due to lack of inversion symmetry center is significant compared with a moderate inter-chain coupling ($J_\perp \sim 0.13$ meV). In this case, the effective staggered field h creating the linear attracting potential is vector sum of that raised by the inter-chain coupling and DM interaction. With the increasing field intensity, the spin-canting effect induced by the DM interaction is strongly enhanced, which is observed from the spectral analysis shown above. The staggered field created by the DM-interaction is also enhanced by increasing the magnetic field ($|\vec{h}_{DM}| \propto |\vec{B}_0 \times \vec{D}|$), leading to the increasing of the attracting energy potential. The increased Néel temperature under magnetic field (See Fig.5 (c)) is also consistent with this suppression of the quantum fluctuations. The crossover from the dominating two-magnon Raman process to three-magnon scattering contributions to the nuclear relaxation may be also related with the magnetic field enhancement of spin-canting effect. At the strong magnetic field side, we fail to observe the field induced spin wave excitation gap as what happens in copper benzoate where the inter-chain coupling is very weak. Based on the Monte Carlo simulations⁵², the threshold for the field strength sufficient to open the energy gap in the spin wave excitations increased mildly with the inter-chain coupling. For the present sample lying in the

1D-3D crossover regime with $J_\perp/J \sim 0.02$, the magnetic field threshold should be much higher than $B_0 = 15.3$ T. Thus, the field induced energy gap of the spin wave excitation is absent in our sample under the present field range. Up to now, we still do not know the physical origin for the $(B_0)^{0.5}$ field dependence of the power-law index and further theoretical calculation is needed.

In quasi-1D quantum spin systems, the magnetic field can be an effective tuning parameter to approach the quantum critical point. In the spin chain system, $\text{NiCl}_2\text{-4SC}(\text{NH}_2)_2$ (DTN) and the spin ladder compound $\text{CuBr}_4(\text{C}_5\text{H}_{12}\text{N})_2$ (BPCB)^{32,33}, the spin excitations at zero field are dominated by magnons with a finite gap, resulting from the single-ion anisotropy and strongly coupled rung. With applied magnetic field, the energy gap between spin-singlets and triplets is tuned linearly to zero due to the competing Zeeman energy in the Hamiltonian. The quantum critical point is approached at B_c . The dominating spin excitations evolve from gapped magnons to spinons in the gapless Luttinger liquid state as seen from NMR studies. Comparatively, we have realized the magnetic field suppression of quantum excitations in the low temperature ordered state in a quasi-1D spin chain system with significant DM-interactions in this study.

To conclude, we have carried out NMR study on a quasi-1D $S = 1/2$ Heisenberg antiferromagnetic chain. The antiferromagnetic long range order is identified from the spectral analysis, and a G -type antiferromagnetism with a ferromagnetic component is proposed. Above T_N , the spinon excitation is observed from the constant $1/T_1$ at low temperatures contributed from the staggered spin susceptibility. At low temperatures well below T_N , the spin lattice relaxation rate $1/T_1$ is observed to flatten out toward zero temperature. By the applied field, $1/T_1$ gradually shows a power-law temperature dependence with the index enhanced from zero to ~ 3 , and finally ~ 5 , which are the typical character for the dominating magnon scattering of the nuclear spins in the conventional 3D classical magnet. The result supplies strong evidence for the magnetic field suppression of quantum magnetic excitations in the magnetically ordered state of the quasi-1D Heisenberg spin chain system. The mechanism for this phenomena is proposed to be related to the enhanced local transverse staggered field generated by the DM interactions under magnetic field.

This research was supported by the National Key Research and Development Program of China (Grant No. 2016YFA0401802 and 2017YFA0303201), the National Natural Science Foundation of China (Grants No. 11504377, 11874057, 11574288, U1732273, U1532153, 11774352, 21301178 and 11674331), 100 Talents Programme of Chinese Academy of Sciences (CAS) and the Major Program of Development Foundation of Hefei Center for Physical Science and Technology (Grant No. 2016FXZY001).

- * Electronic address: hulin@hmfl.ac.cn
 † Electronic address: zhequ@hmfl.ac.cn
 ‡ Electronic address: pili@ustc.edu.cn
- ¹ V. Zapf, M. Jaime, and C. D. Batista, *Rev. Mod. Phys.* **86**, 563 (2014).
 - ² T. Han, J. S. Helton, S. Chu, D. G. Nocera, J. A. Rodriguez-Rivera, C. Broholm, and Y. S. Lee, *Nature (London)* **492**, 406 (2012).
 - ³ M. Punk, D. Chowdhury, and S. Sachdev, *Nat. Phys.* **10**, 289 (2014).
 - ⁴ B. D. Piazza, M. Mourigal, N. B. Christensen, G. J. Nilsen, P. Tregenna-Piggott, T. G. Perring, M. Enderle, D. F. McMorrow, D. A. Ivanov, and H. M. Rønnow, *Nat. Phys.* **11**, 62 (2015).
 - ⁵ P. W. Anderson, *Science* **235**, 1196 (1987).
 - ⁶ S. A. Kivelson, D. S. Rokhsar, and J. P. Sethna, *Phys. Rev. B* **35**, 8865 (1987).
 - ⁷ S. Raghu, X.-L. Qi, C. Honerkamp, and S.-C. Zhang, *Phys. Rev. Lett.* **100**, 156401 (2008).
 - ⁸ C. L. Kane and E. J. Mele, *Phys. Rev. Lett.* **95**, 226801 (2005).
 - ⁹ N. D. Mermin and H. Wagner, *Phys. Rev. Lett.* **17**, 1133 (1966).
 - ¹⁰ H. Bethe, *Z. Phys.* **71**, 205 (1931).
 - ¹¹ D. A. Tennant, R. A. Cowley, S. E. Nagler, and A. M. Tselik, *Phys. Rev. B* **52**, 13368 (1995).
 - ¹² P. R. Hammar, M. B. Stone, D. H. Reich, C. Broholm, P. J. Gibson, M. M. Turnbull, C. P. Landee, and M. Oshikawa, *Phys. Rev. B* **59**, 1008 (1999).
 - ¹³ L. D. Faddeev and L. A. Takhtajan, *Phys. Lett. A* **85**, 375 (1981).
 - ¹⁴ F. D. M. Haldane, *Phys. Rev. Lett.* **66**, 1529 (1991).
 - ¹⁵ M. Mourigal, M. Enderle, A. Klopfferpieper, J.-S. Caux, A. Stunault, and H. M. Ronnow, *Nat. Phys.* **9**, 435 (2013).
 - ¹⁶ B. Lake, D. A. Tennant, C. D. Frost, and S. E. Nagler, *Nat. Mater.* **4**, 329 (2005).
 - ¹⁷ H. J. Schulz, *Phys. Rev. Lett.* **77**, 2790 (1996).
 - ¹⁸ F. H. L. Essler, A. M. Tselik, and G. Delfino, *Phys. Rev. B* **56**, 11001 (1997).
 - ¹⁹ S. K. Satija, J. D. Axe, G. Shirane, H. Yoshizawa, and K. Hirakawa, *Phys. Rev. B* **21**, 2001 (1980).
 - ²⁰ M. T. Hutchings, E. J. Samuelsen, G. Shirane, and K. Hirakawa, *Phys. Rev.* **188**, 919 (1969).
 - ²¹ K. M. Kojima, Y. Fudamoto, M. Larkin, G. M. Luke, J. Merrin, B. Nachumi, Y. J. Uemura, N. Motoyama, H. Eisaki, S. Uchida, et al., *Phys. Rev. Lett.* **78**, 1787 (1997).
 - ²² M. Matsuda, K. Katsumata, K. M. Kojima, M. Larkin, G. M. Luke, J. Merrin, B. Nachumi, Y. J. Uemura, H. Eisaki, N. Motoyama, et al., *Phys. Rev. B* **55**, R11953(R) (1997).
 - ²³ I. A. Zaliznyak, C. Broholm, M. Kibune, M. Nohara, and H. Takagi, *Phys. Rev. Lett.* **83**, 5370 (1999).
 - ²⁴ A. Zheludev, M. Kenzelmann, S. Raymond, E. Ressouche, T. Masuda, K. Kakurai, S. Maslov, I. Tsukada, K. Uchinokura, and A. Wildes, *Phys. Rev. Lett.* **85**, 4799 (2000).
 - ²⁵ I. Tsukada, Y. Sasago, K. Uchinokura, A. Zheludev, S. Maslov, G. Shirane, K. Kakurai, and E. Ressouche, *Phys. Rev. B* **60**, 6601 (1999).
 - ²⁶ A. Zheludev, K. Kakurai, T. Masuda, K. Uchinokura, and K. Nakajima, *Phys. Rev. Lett.* **89**, 197205 (2002).
 - ²⁷ B. Lake, D. A. Tennant, and S. E. Nagler, *Phys. Rev. Lett.* **85**, 832 (2000).
 - ²⁸ B. Lake, D. A. Tennant, and S. E. Nagler, *Phys. Rev. B* **71**, 134412 (2005).
 - ²⁹ A. Zheludev, S. Raymond, L. P. Regnault, F. H. L. Essler, K. Kakurai, T. Masuda, and K. Uchinokura, *Phys. Rev. B* **67**, 134406 (2003).
 - ³⁰ E. G. Sergeicheva, S. S. Sosin, L. A. Prozorova, G. D. Gu, and I. A. Zaliznyak, *Phys. Rev. B* **95**, 020411(R) (2017).
 - ³¹ M. Jeong, H. Mayaffre, C. Berthier, D. Schmidiger, A. Zheludev, and M. Horvatic, *Phys. Rev. Lett.* **118**, 167206 (2017).
 - ³² M. Klanjsek, H. Mayaffre, C. Berthier, M. Horvatic, B. Chiari, O. Piovesana, P. Bouillot, C. Kollath, E. Orignac, R. Citro, et al., *Phys. Rev. Lett.* **101**, 137207 (2008).
 - ³³ S. Mukhopadhyay, M. Klanjsek, M. S. Grbic, R. Blinder, H. Mayaffre, C. Berthier, M. Horvatic, M. A. Continentino, A. Paduan-Filho, B. Chiari, et al., *Phys. Rev. Lett.* **109**, 177206 (2012).
 - ³⁴ F. Casola, T. Shiroka, V. Glazkov, A. Feiguin, G. Dhalenne, A. Revcolevschi, A. Zheludev, H.-R. Ott, and J. Mesot, *Phys. Rev. B* **86**, 165111 (2012).
 - ³⁵ B. Pato-Doldán, L. C. Goómez-Aguirre, A. P. Hansen, J. Mira, S. Castro-García, M. Sánchez-Andújar, M. A. Senñaris-Rodríguez, V. S. Zapf, and J. Singleton, *J. Mater. Chem. C* **4**, 11164 (2016).
 - ³⁶ J. B. Goodenough, *Magnetism and the Chemical Bond* (Interscience (Wiley), New York, 1963).
 - ³⁷ A. Klumper and D. C. Johnston, *Phys. Rev. Lett.* **84**, 4701 (2000).
 - ³⁸ A. M. Clogston and V. Jaccarino, *Phys. Rev.* **121**, 1357 (1961).
 - ³⁹ L. Ma, J. Dai, P. S. Wang, X. R. Lu, Y. Song, C. L. Zhang, G. T. Tan, P. C. Dai, D. Hu, S. L. Li, et al., *Phys. Rev. B* **90**, 144502 (2014).
 - ⁴⁰ L. C. Gomez-Aguirre, B. Pato-Doldan, J. Mira, S. Castro-Garcia, M. A. Senaris-Rodriguez, M. Sanchez-Andujar, J. Singleton, and V. S. Zapf, *J. Am. Chem. Soc.* **138**, 1122 (2016).
 - ⁴¹ C. P. Slichter, *Principles of Magnetic Resonance* (Springer, Berlin, 1990).
 - ⁴² S. Sachdev, *Phys. Rev. B* **50**, 13006 (1994).
 - ⁴³ M. Takigawa, N. Motoyama, H. Eisaki, and S. Uchida, *Phys. Rev. Lett.* **76**, 4612 (1996).
 - ⁴⁴ M. E. Fisher, *Am. J. Phys.* **32**, 343 (1964).
 - ⁴⁵ D. Beeman and P. Pincus, *Phys. Rev.* **166**, 359 (1968).
 - ⁴⁶ D. A. Tennant, T. G. Perring, R. A. Cowley, and S. E. Nagler, *Phys. Rev. Lett.* **70**, 4003 (1993).
 - ⁴⁷ O. V. Misochko, S. Tajima, C. Urano, H. Eisaki, and S. Uchida, *Phys. Rev. B* **53**, R14733(R) (1996).
 - ⁴⁸ A. Zheludev, M. Kenzelmann, S. Raymond, T. Masuda, K. Uchinokura, and S.-H. Lee, *Phys. Rev. B* **65**, 014402 (2001).
 - ⁴⁹ M. Date, H. Yamazaki, M. Motokawa, and S. Tazawa, *Prog. Theor. Phys. Suppl.* **46**, 194 (1970).
 - ⁵⁰ M. Oshikawa and I. Affleck, *Phys. Rev. Lett.* **79**, 2883 (1997).
 - ⁵¹ I. Affleck and M. Oshikawa, *Phys. Rev. B* **60**, 1038 (1999).
 - ⁵² B. Xi, S. J. Hu, J. Z. Zhao, G. Su, B. Normand, and X. Q. Wang, *Phys. Rev. B* **84**, 134407 (2011).

⁵³ D. C. Dender, P. R. Hammar, D. H. Reich, C. Broholm, and G. Aeppli, Phys. Rev. Lett. **79**, 1750 (1997).

⁵⁴ S. A. Zvyagin, E. Cizmar, M. Ozerov, J. Wosnitza, R. Fey-

erherm, S. R. Manmana, and F. Mila, Phys. Rev. B **83**, 060409(R) (2011).